Scratch-induced deformation in fine- and ultrafine-grained bulk alumina

Lin Huang, Zhihui Zhang, Yonghao Zhao, Wenlong Yao,
Amiya K. Mukherjee and Julie M. Schoenung*

Department of Chemical Engineering and Materials Science, University of California – Davis, Davis, CA 95616, USA

The nanoscratch behavior of two bulk α-alumina samples with 1.3 μm and 290 nm average grain sizes, respectively, was investigated using a nanoindenter in scratch mode, in combination with atomic force and scanning electron microscopy. A ductile to brittle transition was observed in the fine-grained sample, while the ultrafine-grained sample exhibited predominantly ductile deformation with a fish-bone feature indicative of a stick–slip mechanism. These findings suggest that grain refinement can increase the potential for plastic deformation in ceramics.
© 2010 Acta Materialia Inc. Published by Elsevier Ltd. All rights reserved.

Scratch tests have been widely used to investigate the wear behavior of ceramic materials during the abrasive machining process. Microscopic observations provide clarity on the crack systems that signify severe brittle fracture during such a scratch test, including lateral, median and radial crack systems [1–10]. The primary mechanisms by which material is removed during brittle fracture include (i) grain dislodgement and (ii) chipping, both of which result from the transformation of flaws at the grain boundaries into intergranular microcracks that propagate under an applied load [3–7,9,11].

Plastic deformation at the micro-scale has also been observed in ceramics, even at room temperature [12–16]. For example, a plastic zone can be produced under the indenter in scratch tests on brittle ceramics [10,13,17,18] and ductile flow can consume much of the energy during the abrasive process [19]. Subsurface damage, such as lateral cracking, intergranular microcracks and intragranular twin/slip bands, have also been observed within the plastic zone in ceramics [20]. In addition, direct observation of slip lines, dislocations and twinning within the plastic zone caused by scratching ceramics has been achieved using transmission electron microscopy (TEM) and high spatial resolution cross-sectional electron microscopy [13,14,16].

When scratching brittle materials with an increasing depth of cut (DOC) the evolution of material deformation can be described as follows: plastic deformation, followed by scale-like cracking and, finally, chipping [17,21]. The position where noticeable cracking occurs along the scratch groove is referred to as the ductile to brittle transition (DBT) point [22]. The existence of a DBT point provides the possibility of machining ceramics at an extremely small DOC in a purely ductile mode by dislocation production and motion, to avoid brittle cracking and subsurface damage [17,22]. In a related work reported by Subhash et al., the authors investigated the variable depth scratch behavior of three different grain size alumina ceramics, with average grain sizes of 2, 15 and 25 μm, respectively. It was determined that the DBT point is a function of scratch parameters, material microstructure and properties [22].

Simplified approaches, such as employing a single grit abrasive scratch, have been employed to study the fundamental scratch behavior of ceramics with average grain sizes in the micron size regime [20,22]. Recently, other related studies have demonstrated the feasibility of utilizing a nanoindenter to study the nanoscratch behavior of various materials [13,14,23–27]. Ghosh et al. successfully employed a nanoindenter in scratch mode to investigate nanoscratch-induced deformation, including microplasticity and microcracking, in a ceramic composite [13,14,27]. In the current research an

* Corresponding author. Tel.: +1 530 752 5840; fax: +1 530 752 9554; e-mail: jmschoenung@ucdavis.edu

MTS nanoindenter XPS system in scratch mode was utilized to investigate the effect of grain size on the nanoscratch behavior of pure bulk α-alumina.

The bulk polycrystalline α-alumina samples were prepared from Taimei powder TM-DAR (~100 nm average grain size, 99.99% purity), using the spark plasma sintering (SPS) (825S DR. SINTER®) technique. The samples were fabricated by controlling the sintering conditions, including the sintering temperature (1350 and 1175 °C, respectively), heating rate (100 °C min⁻¹), holding time (5 and 7 min, respectively) and applied pressure (100 MPa). The as-sintered, bulk samples (19 mm in diameter and 3 mm in thickness) were characterized by X-ray diffraction (XRD) (not shown here) and TEM (see Fig. 1) to verify the composition as pure α-alumina and to determine the average grain sizes (~1.3 μm and ~290 nm, designated samples A-1 and A-2, respectively). The density of each sample (99.1% and 99.6%, respectively) was determined using the Archimedes method. Prior to the nanoscratch tests, the as-sintered samples were carefully polished, using standard diamond polishing techniques, down to a diamond particle size of 1 μm. For the scratch tests a Berkovich nanoindenter tip (tip radius ~20 nm) was employed at a sliding speed of 1 μm s⁻¹, and the scratch direction was aligned along one sharp edge of the triangular pyramid diamond tip in order to ensure geometric consistency in multiple scratch grooves. The normal load was programmed to linearly increase from 100 μN to 200 mN along a scratch length of 200 μm, and the test was repeated 10 times on each sample. The residual scratch tracks were characterized using scanning electron microscopy (SEM) and atomic force microscopy (AFM) after ultrasonic cleaning for 5 min.

The penetration depth profile and the corresponding micrographs of the residual scratch groove morphology for sample A-1 (with an average grain size of 1.3 μm), as well as higher magnification images, are shown in Figure 2. The penetration depth increased to almost 850 nm along the scratch length under the increasing applied normal load. The low-load portion of the penetration depth profile was smooth, with negligible small fluctuations. The appearance of a sudden valley in the profile, which corresponds to the position at which the normal load was ~20 mN and the penetration depth was ~150 nm, indicated the start of brittle fracture in the scratch groove. This position was thus identified as the DBT point. The profile then became irregularly oscillating under continuously increasing load, indicating the occurrence of discontinuous brittle fracture.

The SEM image in Figure 2b illustrates increasing scratch width with load, and the brittle deformation that
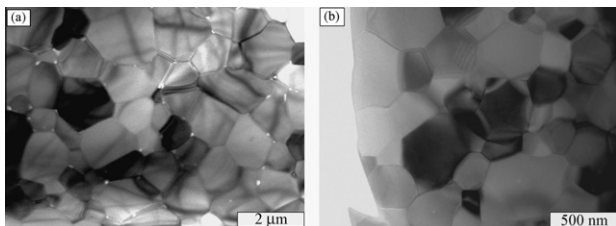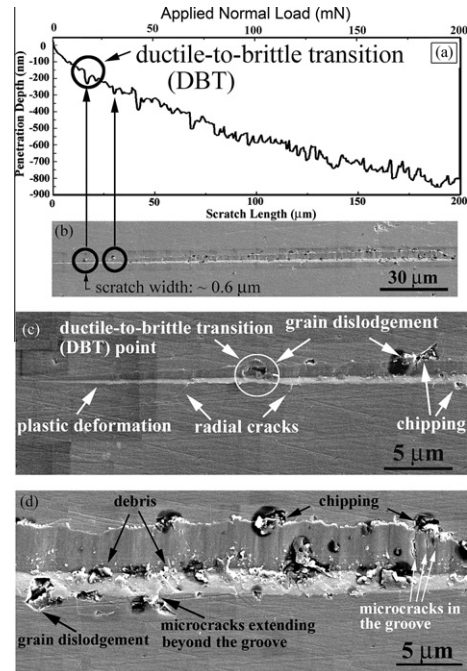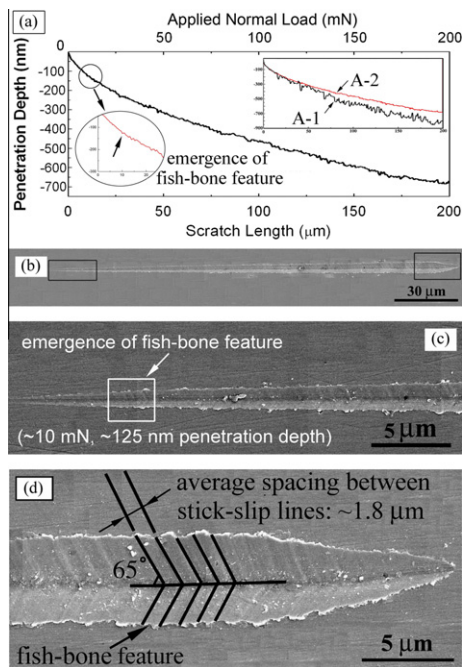

Figure 2. (a) Penetration depth profile for linearly increasing applied normal load to a maximum of 200 mN. (b) SEM image of the corresponding residual scratch path morphology for sample A-1. (c) Magnified view of the low-load region of the scratch. (d) Magnified view of the high-load region of the scratch.

corresponds to the fluctuations in the penetration depth profile can be clearly observed in the image of the residual scratch groove, as indicated by the arrows that link Figure 2a and b. The magnified image of the low-load portion of the scratch in sample A-1 (Fig. 2c) shows the smooth morphology in the region where the penetration depth was small, indicating ductile deformation. Grain dislodgement can be observed at the DBT point. In addition, radial cracks along the scratch can also be observed. In the magnified view of the high-load portion of the scratch (Fig. 2d) typical brittle fracture features can be observed. The more dramatic microscopic damage in this region, which is also reflected in the increased irregularity in the penetration depth profile, is revealed as interrupted material removal, including microcracks both in and extending beyond the groove along grain boundaries, numerous chips and debris and severe grain debonding, dislodgement and grain pull-out caused by intergranular microcracks.

In contrast, sample A-2, which had an ultrafine-grained microstructure (with an average grain size of 290 nm), exhibited a significantly different nanoscratch behavior when tested under identical conditions. The penetration depth profile and the residual scratch morphology for sample A-2 were much smoother compared with those for sample A-1 with a coarser grain size, as shown in Figure 3. From the graph in the upper right-hand corner of Figure 3a, in which the two profiles are shown together, it can be observed that the low-load regions of the two profiles overlap, because both samples experienced elastic–plastic deformation at a very low penetration depth (i.e. DOC) at the beginning of the scratch process when the applied normal load was small. However, after the sample A-1 DBT point, sample A-2

Figure 1. TEM images of alumina samples A-1 and A-2 with average grain sizes of 1.3 μm and 290 nm, respectively.

Figure 3. (a) Penetration depth profile for linearly increasing applied normal load to a maximum of 200 mN. (b) SEM image of the corresponding residual scratch path morphology for sample A-2. (c) Magnified view of the low-load region of the scratch. (d) Magnified view of the high-load region of the scratch.

continued to exhibit elastic–plastic deformation, with only small fluctuations in the profile, while sample A-1 exhibited severe brittle fracture. The apparent differences in the nanoscratch behavior of the two samples can be further quantified by measuring the average fluctuation amplitude in each profile: 63.8 ± 32.0 nm for sample A-1 and 7.9 ± 3.5 nm for sample A-2. The SEM images showing the residual scratch morphology of sample A-2 provide additional evidence of the overall plastic deformation in this ultrafine-grained alumina. The entire scratch was basically smooth, except for some small defects and some attached debris. Upon closer observation of the low- and high-load regions in sample A-2 smeared areas, which may form from grains being pushed aside and piled up during the scratch process, can be seen along the boundaries of the groove. No intergranular or transgranular microcracks or other microscopic damage, such as grain peel-off or pull-out, was observed in or extending beyond the groove. The overall scratch deformation and the corresponding material removal remained in a predominantly ductile mode.

In addition, a fish-bone feature, as shown in Figure 3c, emerged in the scratch groove at the position where the applied normal load was ~10 mN and the penetration depth was ~125 nm, which corresponds to the point in the penetration depth profile at which the emergence of small fluctuations was first observed (see the highlighted region in the bottom left-hand corner of Fig. 3a). The fish-bone feature became more defined with increasing applied normal load along the scratch length. Although there was significant variability in the data, a statistical least squares fit of the fluctuations in the penetration depth profile in Figure 3a (not shown here) indicated that the average spacing between the lines of the fish-bone feature increased with increasing applied normal load, as expected. The average spacing in the high-load region was ~1.8 μm, which is reflected in both the penetration depth profile and the SEM image (Fig. 3d). Furthermore, the angle between the parallel lines of the fish-bone feature and the scratch direction was approximately 65°, which corresponds to the Berkovich tip geometry. Formation of the periodic fish-bone feature may be attributed to the 'stick–slip' mechanism [28], which is in turn due to the competition between static and kinetic friction coefficients during the nanoscratch process [14,18,28–33]. The alternating stick and slip states reflect a change in the way energy is stored [31,33]. Due to the nature of the scratch process, the normal load applied to the indenter tip also generated tangential stresses on the contact surface. Both the normal and induced tangential loads could cause deformation under and in front of the tip. The induced tangential (or shear) stress accumulates in front of the tip when the tip is stuck, and increases with increasing applied normal load, resulting in more and more prominent plastic deformation of the material in front of the tip. At this stage the potential energy is stored due to the work still being done by the equipment. When the stress exceeds the critical stress, the tip slips. At this moment the stored energy is released as kinetic energy, as well as heat caused by friction between the tip and the sample. Then the process repeats itself, which can be detected through the repeated occurrence of small fluctuations in the penetration depth profile (similar fluctuations can also be observed in the induced tangential load profile, not shown here). Furthermore, the shear stress is more concentrated at the pyramidal apex of the tip and gradually decreases along the edge and surface during the stick stage. Therefore, the material right in front of the tip apex should be more deformed, and the fish-bone microstructure thus reflects the shape of the Berkovich tip.

It should be noted that during the nanoscratch testing on sample A-1 stick–slip behavior also occurred, but was difficult to detect because the deformation mode in sample A-1 was dominated by severe brittle fracture, especially at higher applied normal loads. Thus, when the stored energy could not be endured by the sliding strength of the sample, the energy was released, not only as kinetic energy and heat, but also as surface energy through grain dislodgement or the formation of microcracks. Therefore, the potential plastic deformation capability of sample A-1 was dramatically decreased, which is why the fish-bone feature could not be clearly detected on sample A-1 by SEM observation.

The differences in nanoscratch behavior observed for the two alumina samples were further confirmed through comparison of three-dimensional AFM images from the high-load regions of the two scratches, as shown in Figure 4. Pile-up along the grooves was revealed through section analysis for both samples, as shown in the bottom right-hand corners of each image, indicating that both samples had some plastic deformation potential. However, grain dislodgment and a fairly rough groove could be clearly observed for sample A-1, whereas the scratch groove in sample A-2 was relatively smooth. Furthermore, close inspection of Figure 4b reveals the fish-bone
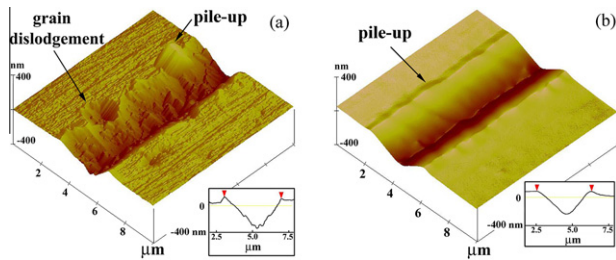
Figure 4. Three-dimensional AFM images and cross-sectional profiles for the high-load region of the scratches in samples (a) A-1 and (b) A-2, respectively.

feature through the contrast in the groove of sample A-2 and the up and down movement of the nanoindenter tip trace. Thus, in combination, the observations described above provide evidence that the bulk alumina sample with ultrafine-grained microstructure had increased potential for plastic deformation.

It has been previously proposed that samples under an indenter tip experience elastic–plastic deformation during the scratch process [10,18]. Based on its crystal structure, the plastic deformation of α-alumina is mainly induced by the activation of dislocation motion in three primary slip systems, i.e. $(0\,0\,0\,1)\frac{1}{3}\langle11\bar{2}0\rangle$ basal slip, $\{11\bar{2}0\}\langle1\bar{1}00\rangle$ prism slip and $\{10\bar{1}1\}\frac{1}{3}\langle\bar{1}101\rangle$ pyramidal slip, even at room temperature [16,34–36]. Therefore, it is deduced that the slip systems in polycrystalline α-alumina may be activated during the scratch process. Due to the ultrafine-grained microstructure in sample A-2, a larger number of grains would be expected to be favorably arranged for the activation of slip systems during the scratch process, as compared with sample A-1 under the same loading conditions, which results in a higher probability of plastic deformation in sample A-2. Further investigation to provide direct evidence of slip system activation in these materials is ongoing.

Scratch penetration profiles and SEM and AFM images illustrate different nanoscratch behavior in two bulk polycrystalline α-alumina samples with 1.3 μm and 290 nm average grain sizes, respectively, under a linearly increasing loading condition using a nanoindenter XPS system in scratch mode. A DBT was observed at low loads in the coarser grained alumina sample. At higher loads this sample exhibited radial cracks, grain dislodgement and microcracks, which are typical features associated with brittle deformation. In contrast, the scratch behavior in the finer grained alumina sample remained in a predominantly ductile mode, demonstrating an increased potential for plastic deformation. A fish-bone feature was observed in the scratch groove of the finer grained alumina, indicating that the stick–slip mechanism was also operable in this material.

[1] M. Klecka, G. Subhash, Wear 265 (2008) 612.
[2] S.K. Lee, R. Tandon, M.J. Readey, B.R. Lawn, J. Am. Ceram. Soc. 83 (2000) 1428.
[3] H.H.K. Xu, S. Jahanmir, J. Mater. Sci. 30 (1995) 2235.
[4] H.H.K. Xu, S. Jahanmir, Wear 192 (1996) 228.
[5] H.H.K. Xu, S. Jahanmir, L.K. Ives, J. Mater. Res. 11 (1996) 1717.
[6] H.H.K. Xu, S. Jahanmir, Y.S. Wang, J. Am. Ceram. Soc. 78 (1995) 881.
[7] H.H.K. Xu, N.P. Padture, S. Jahanmir, J. Am. Ceram. Soc. 78 (1995) 2443.
[8] H.H.K. Xu, L.H. Wei, S. Jahanmir, J. Mater. Res. 10 (1995) 3204.
[9] H.H.K. Xu, L.H. Wei, S. Jahanmir, J. Am. Ceram. Soc. 79 (1996) 1307.
[10] X.N. Jing, S. Maiti, G. Subhash, J. Am. Ceram. Soc. 90 (2007) 885.
[11] G. Subhash, R. Bandyo, J. Am. Ceram. Soc. 88 (2005) 918.
[12] D. Ghosh, G. Subhash, N. Orlovskaya, Scripta Mater. 62 (2010) 839.
[13] D. Ghosh, G. Subhash, G.R. Bourne, Scripta Mater. 61 (2009) 1075.
[14] D. Ghosh, G. Subhash, R. Radhakrishnan, T.S. Sudarshan, Acta Mater. 56 (2008) 3011.
[15] J.M. Staehler, W.W. Predebon, B.J. Pletka, G. Subhash, Mater. Sci. Eng. 291A (2000) 37.
[16] B.J. Inkson, Acta Mater. 48 (2000) 1883.
[17] G. Subhash, J.E. Loukus, S.M. Pandit, Mech. Mater. 34 (2002) 25.
[18] Y. Ahn, T.N. Farris, S. Chandrasekar, Mech. Mater. 29 (1998) 143.
[19] T.W. Hwang, C.J. Evans, S. Malkin, Wear 229 (1999) 862.
[20] G. Subhash, M.A. Marszalek, S. Maiti, J. Am. Ceram. Soc. 89 (2006) 2528.
[21] K. Li, T.W. Liao, J. Mater, Process. Tech. 57 (1996) 207.
[22] G. Subhash, M. Klecka, J. Am. Ceram. Soc. 90 (2007) 3704.
[23] B.D. Beake, G.A. Bell, S.R. Goodes, N.J. Pickford, J.F. Smith, Surf. Eng. 26 (2010) 37.
[24] Y.Q. Wu, H. Huang, J. Zou, J.M. Dell, J. Vac. Sci. Tech. B 27 (2009) 1374.
[25] P. Tordjeman, N. Morel, M. Ramonda, Appl. Surf. Sci. 255 (2009) 6999.
[26] P.C. Wo, I.P. Jones, A.H.W. Ngan, Philos. Mag. 88 (2008) 1369.
[27] D. Ghosh, G. Subhash, N. Orlovskaya, Acta Mater. 56 (2008) 5345.
[28] Q. Yuan, N. Ramisetti, R.D.K. Misra, Acta Mater. 56 (2008) 2089.
[29] K. Li, Y. Shapiro, J.C.M. Li, Acta Mater. 46 (1998) 5569.
[30] D. Mulliah, S.D. Kenny, E. Mcgee, R. Smith, A. Richter, B. Wolf, Nanotechnology 17 (2006) 1807.
[31] S.D. Kenny, D. Mulliah, C.F. Sanz-Navarro, R. Smith, Philos. Trans. R. Soc. A 363 (2005) 1949.
[32] R. Smith, D. Mulliah, S.D. Kenny, E. McGee, A. Richter, M. Gruner, Wear 259 (2005) 459.
[33] D. Mulliah, S.D. Kenny, R. Smith, Phys. Rev. B 69 (2004).
[34] J. Castaing, A. Munoz, D.G. Garcia, A.D. Rodriguez, Mater. Sci. Eng. 233A (1997) 121.
[35] A. Nakamura, T. Yamamoto, Y. Ikuhara, Acta Mater. 50 (2002) 101.
[36] N. Shibata, M.F. Chisholm, A. Nakamura, S.J. Pennycook, T. Yamamoto, Y. Ikuhara, Science 316 (2007) 82.